Computational Study on the Effects of Mechanical Constraint on the Performance of Si Nanosheets as Anode Materials for Lithium-Ion Batteries

Qifang Yin[1], Zhenbin Guo[1], Yinfeng Li[1,2,3], Haimin Yao[1,*]

[1]Department of Mechanical Engineering, The Hong Kong Polytechnic University, Hung Hom, Kowloon, Hong Kong

[2]Department of Engineering Mechanics, School of Naval Architecture, Ocean and Civil Engineering (State Key Laboratory of Ocean Engineering), Shanghai Jiao Tong University, Shanghai 200240, China

[3]Key Laboratory of Hydrodynamics (Ministry of Education), Shanghai Jiao Tong University, Shanghai 200240, China

ABSTRACT

Lithiation process of Si has been widely studied, while most of the previous works neglected the effects of mechanical constraint from the accessory materials such as binder and conductive additive on the Si. In this paper, we carry out molecular dynamics simulations to investigate the effects of mechanical constraint on the performances, such as capacity and lithiation rate, of Si nanosheets as the anode material for lithium-ion batteries. Our results show that strong mechanical constraint would largely affect the capacity and lithiation rate of Si nanosheets. Remedial strategies for improving the capacity and lithiation rate of the constrained Si nanosheets are proposed, giving rise to guidelines for the design of Si-based anode material for high-performance lithium-ion batteries.

1. INTRODUCTION

Silicon (Si) is deemed as one of the most promising anode materials for the next-generation lithium-ion batteries (LIBs) due to its extraordinarily high capacity, while the huge volume change during lithiation and delithiation processes and the consequent rapid degradation of electrochemical performance impede its wider application. Similar problem was also encountered by other anode materials with high theoretical capacity such as SnO_2.[1] To make the best use of the high capacity of Si and meanwhile prohibit the side-effects of volume change, considerable efforts have been devoted to the studies on the mechanical behaviors of Si in cycling.[2-7] For example, Bower *et al*. theoretically analyzed the Li-ion concentration and the resulting stress field in Si during the lithiation process.[8] Liu *et al*. accounted for the size-dependent fracture of Si nano-particle during lithiation using an elastic and perfectly-plastic model.[9] However, most of these analyses apply to free-standing Si particles. In fact, Si nanomaterials as the active material to accommodate Li-ions are normally embedded in a matrix of accessory materials including binder and conductive additive such as carbon black. The effects of the matrix especially its mechanical properties on the performance of Si-based electrode are still unclear and sometimes even contradictory. For example, Li *et al*. compared the electrochemical performances of crystalline Si powder in two binders with distinct mechanical properties.[10] It was found that the Si electrode performed much better when an extremely stiff and brittle polymer was used as binder. In contrast, Liu *et al*. successfully improved the cyclability of Si particles by using a soft and compliant elastomeric binder.[11] Moreover, two-dimensional Si nanosheets, with the use of different binders, were found to exhibit distinct capacities (~1500 mAh g^{-1}, and ~865 mAh g^{-1})[12,13], implying the important role played by the accessory materials. For a better understanding of the alloying process of Si, the effects of

mechanical constraint on lithiation were investigated. For instance, Wang *et al*. simulated the lithiation and delithiation processes of a substrate-constrained Si film. An asymmetric rate behavior was found, which was attributed to the opposite directions of stress developed during lithiation and delithiation.[14] Using finite element analysis, Xu and Zhao found that the evolution of lithiation-induced stress in a single particle anode embedded in a matrix is quite different from that in a free-standing counterpart.[15]

Despite these progresses, the effects of mechanical constraint on the performance of Si-based electrodes are still unclear. In this paper, we apply the molecular dynamics (MD) simulations to investigate the performance of the mechanically constrained Si-based anode, including the mass capacity and the lithiation rate. Our study will be mainly focused on Si nanosheets rather than particles because the large active surface area and small thickness (less than 10 nm) of nanosheets would result in a high lithiation/delithiation rate[16-17] and stable solid electrolyte interphase (SEI) layer[12]. More importantly, a method for fabricating mass Si nanosheets was recently developed implying a great promise of Si nanosheets as an anode material for LIBs.[12, 18]

2. MODELING AND COMPUTATIONAL DETAILS

When preparing electrode for LIBs, active materials such as Si nanosheets normally are mixed with accessory materials including binder (*e.g.* sodium alginate), conductive additive (*e.g.* carbon black) and solvent (*e.g.*, DI water). The obtained slurry is then uniformly spread on a current collector and dried for use. Clearly, in such a composite electrode material, the Si nanosheets are not free-standing. Instead, they are embedded in a composite matrix consisting of binder and carbon black with structure schematically shown in Figure 1a. During the lithiation and delithiation process, the volume change of the Si nanosheets will be mechanically

constrained by the surrounding accessory materials. Consequently, the performance of the Si in the electrode might be affected.

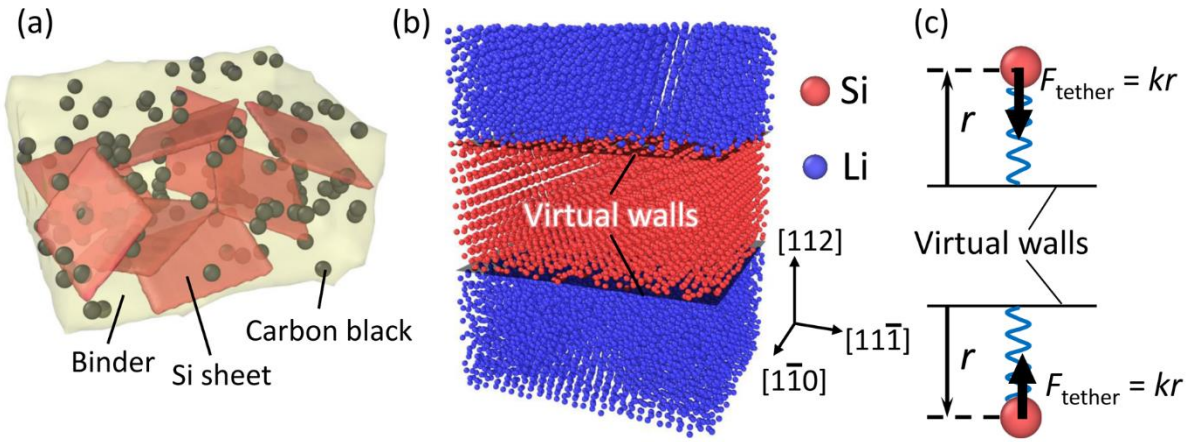

Figure 1. (a) Schematics of the structure of anode composite consisting of Si nanosheet as the active material, sodium alginate as the binder and carbon black as the conductive additive. (b) Illustration of the MD model. The gray planes indicate the position of the virtual walls used to model the mechanical constraint applied on Si. (c) To simulate the mechanical constraint from the surrounding accessory materials, virtual tethering forces are applied on the Si atoms that cross the virtual walls.

To estimate the effect of mechanical constraint on the lithiation of Si nanosheet, an MD model was constructed to simulate the lithiation process of Si nanosheet. Figure 1b shows the unit cell of the model which includes a Si nanosheet sandwiched by two thick Li plates. Originally, the Si sheet is single crystalline with in-plane dimensions equal to 7.3 nm and 6.2 nm along [11$\bar{1}$] and [1$\bar{1}$0] directions, respectively. Periodic boundary conditions are applied along the in-plane directions. Lithiation takes place along [112] direction, which is the out-of-plane direction of the Si nanosheet. Three different thicknesses of the Si sheet are considered including 3.6 nm, 4.3 nm, and 5.0 nm. Due to the limitation of MD simulation, here accessory materials including binder and carbon black are not constructed in our simulation model, but their mechanical constraint to the Si nanosheet is considered by introducing two virtual walls situated at the surfaces of Si sheets before lithiation, as shown in Figure 1b. During lithiation, Si atoms on the surface that cross the virtual reference walls are assumed to experience tethering force given

by $F_{\text{tether}} = kr$, where k is the spring constant of the virtual tether and r stands for the distance from the corresponding virtual wall, as illustrated in Figure 1c. As a parameter characterizing the intensity of mechanical constraint, the order of magnitude of k can be estimated using a simple sandwich model shown in Figure 2a. Here, the surrounding accessory materials are modeled as particle-reinforced composite plates whose mechanical properties can be estimated by a 2D representative volume element (RVE) model shown in Figure 2b. The original thicknesses of the Si nanosheet and the surrounding plates are denoted as h_0 and λh_0, respectively. The ratio λ can be roughly taken as half of the volumetric ratio between the accessory materials and Si sheets.

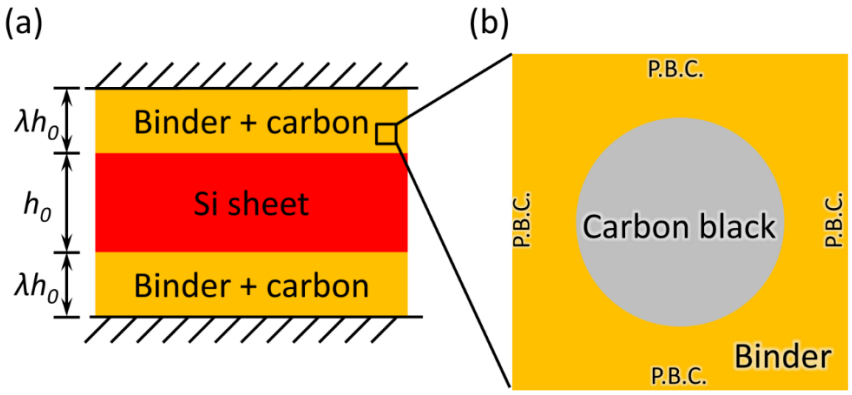

Figure 2. (a) Simplified model of anode consisting of Si nanosheets embedded in a composite matrix. (b) Representative volume element model of the composite accessory materials consisting of binder and carbon black, P.B.C.: periodic boundary condition.

Let the Si nanosheet have a virtual uniform expansion along the thickness direction, which results in a displacement of the surface of the nanosheet into the accessory material, denoted as Δr. If the surfaces of the surrounding plates are fixed (as shown in Figure 2a), the force experienced by a single Si atom on the surface is $A_0 E \Delta r / \lambda h_0$, where E is the effective elastic modulus of the composite matrix and A_0 is the sectional area of a single Si atom. Therefore, the derivative of the force with respect to the displacement, which represents the spring constant k, is given by

$$k = \frac{EA_0}{\lambda h_0} \quad (1)$$

In Eq. (1), the upper and lower bounds of the effective elastic modulus E of the composite matrix can be estimated through the rule of mixture

$$E_{\text{upper}} = E_{\text{b}}V_{\text{b}} + E_{\text{c}}V_{\text{c}}$$

$$E_{\text{lower}} = \frac{E_{\text{b}}E_{\text{c}}}{E_{\text{b}}V_{\text{c}} + E_{\text{c}}V_{\text{b}}}$$

where E_{b} and E_{c} are the elastic moduli of binder and carbon black, and V_{b} and V_{c} are the volume fractions of them. Taking the mass ratio between binder and carbon black as 1:1, and the densities of binder (e.g., sodium alginate) and carbon black as 1.6 g cm^{-3} and 2.3 g cm^{-3} respectively, the volumetric ratio between them is estimated to be 6:4. Taking the Young's moduli of the binder (sodium alginate) and carbon black as 2.7 GPa and 100 GPa respectively,[19] the upper and lower bounds of the effective elastic modulus are estimated to be 42.6 GPa and 4.5 GPa. For a more precise prediction, we carry out Finite Element Analysis (FEA) (see Supporting Information). The result of the FEA simulation shows that the effective elastic modulus is around 7 GPa. This will be used as the typical value of the composite matrix in the following discussion. For a real electrode, if the mass ratio between Si/carbon black/sodium alginate is 3:1:1 and the densities of Si, sodium alginate and carbon black are 2.3 g cm^{-3}, 1.6 g cm^{-3} and 2.3 g cm^{-3} respectively, λ can be estimated to be 0.4. Substituting E = 7 GPa and $\lambda = 0.4$ into Eq. (1) and taking A_0 = 7 Å² and h_0 = 4 nm, k is estimated to be around 0.3 N m^{-1}. In our MD simulations, various values of k ranging from 10^{-3} to 10^{3} N m^{-1} are considered to study the effect of mechanical constraint on the lithiation of Si nanosheets. MD simulation is carried out by using the Large-scale Atomic/Molecular Massively Parallel Simulator (LAMMPS)[20] with charge equilibrium package[21-23]. The interatomic relationship between Si and Li is described by the

reactive force field (ReaxFF) potential,[24] which has been demonstrated applicable for simulating the process of alloying between Li and Si.[24-31]. LAMMPS command "fix wall/harmonic" [20] is applied with the associated spring constant taken as the value of k under investigation. The temperature in all simulations is set as 300 K with Berendsen thermostat[32] and time step is taken as 2 fs. The mass capacity C of the anodes is computed through

$$C_{\mathrm{m}} = \frac{N_{\mathrm{Li}} e_0}{m_{\mathrm{Si}}} \tag{2}$$

where N_{Li} is the number of Li atoms that have been inserted into the Si,[31] e_0 the electron charge and m_{Si} the mass of the Si. Lithiation is deemed as completed if the ratio between the numbers of Li-ions and Si atoms reaches 4.4 or the number of inserted Li atoms changes less than 1% within 10000 MD steps. The open visualization tool (OVITO)[33] is applied for post-processing and visualization.

3. RESULTS AND DISCUSSION

Figure 3a depicts the snapshots of a free-standing Si nanosheet (k = 0) at different lithiation extents. Here, the lithiation extent is characterized by the ratio of the number of inserted Li-ions to that at full lithiation when lithiated Si is assumed to have formula $Li_{4.4}Si$ with the corresponding mass capacity equal to 4200 mAh g^{-1}. During the simulated lithiation process, a sharp boundary between the lithiated and unlithiated regions is observed, which is consistent with the previous results.[28, 34-36] Figure 3b shows the normalized mass capacities as a function of k for different sheet thicknesses. Under weak constraint with $k \leq 10^{-2}$ N m^{-1}, full lithiation can be achieved; while under strong constraint with $k \geq 10$ N m^{-1}, partial lithiation (~20%) is achieved, giving rise to capacity around ~800 mAh/g. For a real case with mass ratio between Si/carbon

black/binder is 3:1:1, k has been estimated to be around 0.3 N m^{-1} which, according to Figure 3b, would lead to partial lithiation (~50%) and capacity around 2000 mAh/g. For an electrode with mass ratio between Si/carbon black/binder is 8:1:1, k is around 1.0 N m^{-1} which, according to Figure 3b, leads to capacity as low as 1400 mAh/g. This may explain the phenomenon that high mass loading of Si usually affects the performance of electrode.[37] Compared to sodium alginate, other binders such as polyvinylidene fluoride (PVDF) and carboxymethyl cellulose (CMC) have comparable density but lower Young's moduli (200-400 MPa for PVDF[38-39] and ~1.0 GPa for CMC[10]), resulting in less mechanical constraint and therefore higher mass capacity. Meanwhile, Figure 3b compares the capacities of Si nanosheets with different thicknesses. It can be seen that capacity exhibits little dependence on the thickness within the discussed range. This is consistent with the earlier finding that thickness-dependent capacity occurs only when thickness is relatively large (> 50 nm).[40-42] Figure 3c shows the lithiation extents reached within a prescribed time (52.6 ps in MD time, which is the time when the 3.6 nm thick, non-constrained Si nanosheet reaches full lithiation). Figure S3 (see Supporting Information) plots the migration velocity of the phase boundary[43] as a function of the constraint intensity within the initial 20 ps of lithiation. It can be seen that Si nanosheet under stronger constraint reaches lower-leveled lithiation, implying that mechanical constraint would reduce the diffusivity of Li-ion in Si and therefore reduce the lithiation rate. Meanwhile, the lithiation rate, unlike the capacity, exhibits a strong dependence on the sheet thickness. For example, under constraint with k = 0.1 N m^{-1} which is close to our estimation for the realistic cases, a sheet of 5.0 nm thick achieves ~47% lithiation in 52.6 ps (MD time), while a 3.6 nm thick sheet reaches ~74% lithiation in the same time. These results indicate that thickness can also effectively affect the diffusivity of Li in Si of the anode material. Under the same constraint, larger thickness leads to smaller Li diffusivity. This can be understood

because thicker sheet would lead to larger change in thickness and therefore experience higher compressive stress from the accessory materials, resulting in smaller Li diffusivity.[43]

Based on above simulation results, two remedial strategies can be proposed to improve the performance of the Si nanosheet anode: one is to choose softer binder and the other one to reduce the thickness of Si nanosheets.

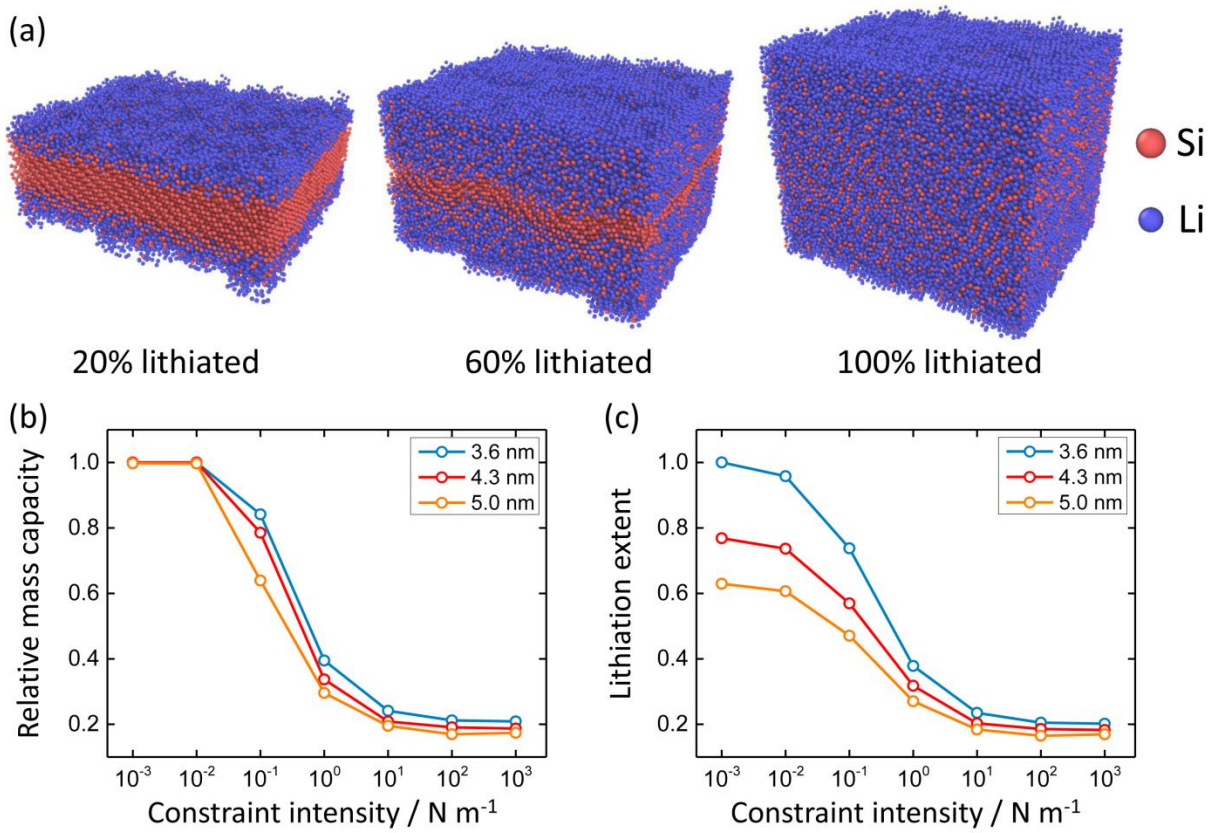

Figure 3. (a) Snapshots of a free-standing (k = 0) Si nanosheet at different lithiation extents. (b) Normalized mass capacity (by the theoretical value 4200 mAh g^{-1}) as a function of constraint parameter k. (c) Lithiation extent achieved within a given MD time.

It is worth noting in Figure 3b that the relative mass capacities reach a steady value when the constraint intensity is relatively large (> 10^2 N m^{-1}). This trend implies that lithiation can always happen regardless of the magnitude of the constraint intensity, and there exists a minimum capacity even for very large constraint intensity. This phenomenon may be attributed to the facile

lithiation of the surface sites of Si (see Figure S4 in the Supporting Information),[44] which, in turn, manifests the promise of Si nanosheet due to its high surface area. The effects of the mechanical constraint on the lithiation time and Li diffusivity may help in understanding the relationship between the constraint intensity and the impedance of the electrode material.[45-46]

Considering that the mechanical constraint takes effect when the volume of Si varies during lithiation, the effect of constraint on the performance can be greatly reduced if the lithiation-induced volume change of Si can be absorbed. This might be achieved by introducing porosity into the Si sheets. To examine the effect of porosity on easing the side effects of mechanical constraint, above MD simulations are repeated on a porous Si sheet containing a through-hole in the center, as shown in Figure 4a. Holes with diameters ranging from 1 nm to 5 nm are considered, and the corresponding porosity varied from 1.7% to 45%. The thickness of the sheets is fixed at 3.6 nm. The calculated mass capacity is plotted in Figure 4b as a function of porosity for k = 0.1~100 N m^{-1}. As expected, higher porosity gives rise to higher mass capacity, irrespective of the external mechanical constraint. Therefore, the side effect of mechanical constraint can be alleviated by introducing porosity. For example, for a Si sheet under constraint with k = 0.1 N m^{-1}, the mass capacity can reach that of an unconstrained counterpart if porosity of 28% or even higher is introduced. Although larger porosity is beneficial for higher mass capacity, it may not be necessarily preferred if volumetric capacity matters. Figure 4c shows the variation of the volumetric capacity C_{V} with the porosity. Different from the mass capacity, the volumetric capacity does not monotonically increase with the porosity. This is because the volumetric capacity $C_{\mathrm{V}} = C_{\mathrm{m}} \times \rho$, where ρ denotes the apparent density of the porous Si. As the porosity increases, the mass capacity C_{m} increases while the apparent density of porous Si ρ decreases. There exists an optimal porosity around 10% for k = 0.1 N m^{-1} for example, at which

the maximum volumetric capacity is achieved. For the cases with higher constraint such as k =10 and 100 N m^{-1}, such optimal porosity may also exist even though it is not observed in the more practically meaningful range of porosity as shown in Figure 4c. Therefore, higher porosity may not necessarily lead to higher volumetric capacity especially when the external constraint is weak.

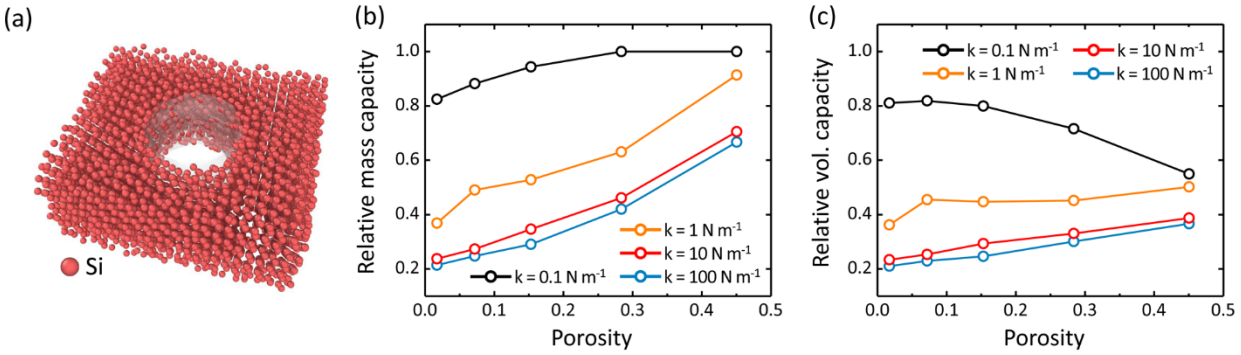

Figure 4. (a) Simulation model of porous Si nanosheet, (b) relative mass capacity and (c) relative volumetric capacity of the constrained porous Si nanosheet with different porosities.

4. CONCLUSIONS

In this study, the effects of the mechanical constraint from the matrix of carbon black and binder on the performances of Si nanosheet anode material were investigated by MD simulation. Results show that large mechanical constraint can reduce the mass capacity and lithiation rate of Si nanosheets. Based on the calculations, we propose following approaches to improve the performance of the Si nanosheet anode material in the constraining matrix: (1) choosing a softer binder material, (2) reducing the thickness of the Si nanosheet, and (3) introducing porous structure. In addition, with the usage of binder materials, the porosity of porous Si anode should be designed cautiously to avoid a possible reduction in volumetric capacity. Although the results are derived on the basis of Si, it can be generalized to the other electrode materials that also experience large volume expansion during alloying with Li, such as Ge, Sn, SnO_2, or even

cathode materials. We believe that our results can serve as a useful guideline for the design and fabrication of the Si-based electrode materials for the next-generation LIBs.

ASSOCIATED CONTENT

Supporting Information

Strain-stress curves of sodium alginate, the effective modulus of accessory material, the migration velocity of the phase boundary, and the atomic configuration after lithiation with large constraint

AUTHOR INFORMATION

Corresponding Author

*E-mail: mmhyao@polyu.edu.hk

Notes

The authors declare no competing financial interest.

ACKNOWLEDGMENTS

This work was supported by the General Research Fund (GRF) from the Research Grant Council of Hong Kong (Grant No. PolyU 152064/15E).

REFERENCES

1. Li, Q. Q.; Li, W. Q.; Feng, Q.; Wang, P.; Mao, M. M.; Liu, J. B.; Zhou, L. M.; Wang, H. T.; Yao, H. M., Thickness-Dependent Fracture of Amorphous Carbon Coating on SnO_2 Nanowire Electrodes. *Carbon* **2014**, *80*, 793-798.
2. Bower, A. F.; Guduru, P. R., A Simple Finite Element Model of Diffusion, Finite Deformation, Plasticity and Fracture in Lithium Ion Insertion Electrode Materials. *Modell. Simul. Mater. Sci. Eng.* **2012**, *20*, 045004.
3. Golmon, S.; Maute, K.; Lee, S. H.; Dunn, M. L., Stress Generation in Silicon Particles During Lithium Insertion. *Appl. Phys. Lett.* **2010**, *97*, 033111.
4. Zhao, K. J.; Pharr, M.; Wan, Q.; Wang, W. L.; Kaxiras, E.; Vlassak, J. J.; Suo, Z. G., Concurrent Reaction and Plasticity During Initial Lithiation of Crystalline Silicon in Lithium-Ion Batteries. *J. Electrochem. Soc.* **2012**, *159*, A238-A243.

5. Ma, Z. S.; Li, T. T.; Huang, Y. L.; Liu, J.; Zhou, Y. C.; Xue, D. F., Critical Silicon-Anode Size for Averting Lithiation-Induced Mechanical Failure of Lithium-Ion Batteries. *RSC Adv.* **2013**, *3*, 7398-7402.
6. Haftbaradaran, H.; Song, J.; Curtin, W. A.; Gao, H. J., Continuum and Atomistic Models of Strongly Coupled Diffusion, Stress, and Solute Concentration. *J. Power Sources* **2011**, *196*, 361-370.
7. Stein, P.; Xu, B., 3d Isogeometric Analysis of Intercalation-Induced Stresses in Li-Ion Battery Electrode Particles. *Comput. Methods. Appl. Mech. Eng.* **2014**, *268*, 225-244.
8. Bower, A. F.; Guduru, P. R.; Chason, E., Analytical Solutions for Composition and Stress in Spherical Elastic-Plastic Lithium-Ion Electrode Particles Containing a Propagating Phase Boundary. *Int. J. Solids Struct.* **2015**, *69-70*, 328-342.
9. Liu, X. H.; Zhong, L.; Huang, S.; Mao, S. X.; Zhu, T.; Huang, J. Y., Size-Dependent Fracture of Silicon Nanoparticles During Lithiation. *ACS Nano* **2012**, *6*, 1522-1531.
10. Li, J.; Lewis, R. B.; Dahn, J. R., Sodium Carboxymethyl Cellulose - a Potential Binder for Si Negative Electrodes for Li-Ion Batteries. *Electrochem. Solid-State Lett.* **2007**, *10*, A17-A20.
11. Liu, W. R.; Yang, M. H.; Wu, H. C.; Chiao, S. M.; Wu, N. L., Enhanced Cycle Life of Si Anode for Li-Ion Batteries by Using Modified Elastomeric Binder. *Electrochem. Solid-State Lett.* **2005**, *8*, A100-A103.
12. Zhang, X. H.; Qiu, X. Y.; Kong, D. B.; Zhou, L.; Li, Z. H.; Li, X. L.; Zhi, L. J., Silicene Flowers: A Dual Stabilized Silicon Building Block for High-Performance Lithium Battery Anodes. *ACS Nano* **2017**, *11*, 7476-7484.
13. Ryu, J.; Hong, D.; Choi, S.; Park, S., Synthesis of Ultrathin Si Nanosheets from Natural Clays for Lithium-Ion Battery Anodes. *ACS Nano* **2016**, *10*, 2843-2851.
14. Wang, M.; Xiao, X. R., Investigation of the Chemo-Mechanical Coupling in Lithiation/Delithiation of Amorphous Si through Simulations of Si Thin Films and Si Nanospheres. *J. Power Sources* **2016**, *326*, 365-376.
15. Xu, R.; Zhao, K. J., Mechanical Interactions Regulated Kinetics and Morphology of Composite Electrodes in Li-Ion Batteries. *Extreme Mech. Lett.* **2016**, *8*, 13-21.
16. Liu, J. H.; Liu, X. W., Two-Dimensional Nanoarchitectures for Lithium Storage. *Adv. Mater.* **2012**, *24*, 4097-4111.
17. Kulish, V. V.; Malyi, O. I.; Ng, M. F.; Wu, P.; Chen, Z., Enhanced Li Adsorption and Diffusion in Silicon Nanosheets Based on First Principles Calculations. *RSC Adv.* **2013**, *3*, 4231-4236.
18. Lang, J. L.; Ding, B.; Zhang, S.; Su, H. X.; Ge, B. H.; Qi, L. H.; Gao, H. J.; Li, X. Y.; Li, Q. Y.; Wu, H., Scalable Synthesis of 2D Si Nanosheets. *Adv. Mater.* **2017**, *29*, 1701777.
19. Robertson, J., Diamond-Like Amorphous Carbon. *Mater. Sci. Eng., R* **2002**, *37*, 129-281.
20. Plimpton, S., Fast Parallel Algorithms for Short-Range Molecular-Dynamics. *J. Comput. Phys.* **1995**, *117*, 1-19.
21. Aktulga, H. M.; Fogarty, J. C.; Pandit, S. A.; Grama, A. Y., Parallel Reactive Molecular Dynamics: Numerical Methods and Algorithmic Techniques. *Parallel Comput.* **2012**, *38*, 245-259.
22. Rappe, A. K.; Goddard III, W. A., Charge Equilibration for Molecular Dynamics Simulations. *J. Phys. Chem.* **1991**, *95*, 3358-3363.
23. Nakano, A., Parallel Multilevel Preconditioned Conjugate-Gradient Approach to Variable-Charge Molecular Dynamics. *Comput. Phys. Commun.* **1997**, *104*, 59-69.
24. Ostadhossein, A.; Cubuk, E. D.; Tritsaris, G. A.; Kaxiras, E.; Zhang, S.; van Duin, A. C., Stress Effects on the Initial Lithiation of Crystalline Silicon Nanowires: Reactive Molecular Dynamics Simulations Using Reaxff. *Phys. Chem. Chem. Phys.* **2015**, *17*, 3832-40.
25. Kim, S. Y.; Ostadhossein, A.; van Duin, A. C.; Xiao, X.; Gao, H.; Qi, Y., Self-Generated Concentration and Modulus Gradient Coating Design to Protect Si Nano-Wire Electrodes During Lithiation. *Phys. Chem. Chem. Phys.* **2016**, *18*, 3706-15.
26. Jung, H.; Lee, M.; Yeo, B. C.; Lee, K. R.; Han, S. S., Atomistic Observation of the Lithiation and Delithiation Behaviors of Silicon Nanowires Using Reactive Molecular Dynamics Simulations. *J. Phys. Chem. C* **2015**, *119*, 3447-3455.

27. Kim, K. J.; Qi, Y., Vacancies in Si Can Improve the Concentration-Dependent Lithiation Rate: Molecular Dynamics Studies of Lithiation Dynamics of Si Electrodes. *J. Phys. Chem. C* **2015**, *119*, 24265-24275.
28. Kim, S. P.; Datta, D.; Shenoy, V. B., Atomistic Mechanisms of Phase Boundary Evolution During Initial Lithiation of Crystalline Silicon. *J. Phys. Chem. C* **2014**, *118*, 17247-17253.
29. Lee, H. S.; Lee, B. J., Structural Changes During Lithiation and Delithiation of Si Anodes in Li-Ion Batteries: A Large Scale Molecular Dynamics Study. *Met. Mater. Int.* **2014**, *20*, 1003-1009.
30. Wang, X., et al., High Damage Tolerance of Electrochemically Lithiated Silicon. *Nat. Commun.* **2015**, *6*, 8417.
31. Kim, K. J.; Wortman, J.; Kim, S. Y.; Qi, Y., Atomistic Simulation Derived Insight on the Irreversible Structural Changes of Si Electrode During Fast and Slow Delithiation. *Nano Lett.* **2017**, *17*, 4330-4338.
32. Berendsen, H. J. C.; Postma, J. P. M.; Vangunsteren, W. F.; Dinola, A.; Haak, J. R., Molecular-Dynamics with Coupling to an External Bath. *J. Chem. Phys.* **1984**, *81*, 3684-3690.
33. Stukowski, A., Visualization and Analysis of Atomistic Simulation Data with Ovito-the Open Visualization Tool. *Modell. Simul. Mater. Sci. Eng.* **2010**, *18*, 015012.
34. Liu, X. H., et al., In Situ Atomic-Scale Imaging of Electrochemical Lithiation in Silicon. *Nat. Nanotechnol.* **2012**, *7*, 749-756.
35. McDowell, M. T.; Lee, S. W.; Harris, J. T.; Korgel, B. A.; Wang, C. M.; Nix, W. D.; Cui, Y., In Situ TEM of Two-Phase Lithiation of Amorphous Silicon Nanospheres. *Nano Lett.* **2013**, *13*, 758-764.
36. McDowell, M. T.; Ryu, I.; Lee, S. W.; Wang, C. M.; Nix, W. D.; Cui, Y., Studying the Kinetics of Crystalline Silicon Nanoparticle Lithiation with in Situ Transmission Electron Microscopy. *Adv. Mater.* **2012**, *24*, 6034-6041.
37. Karkar, Z.; Mazouzi, D.; Hernandez, C. R.; Guyomard, D.; Roue, L.; Lestriez, B., Threshold-Like Dependence of Silicon-Based Electrode Performance on Active Mass Loading and Nature of Carbon Conductive Additive. *Electrochim. Acta* **2016**, *215*, 276-288.
38. Mendoza, H.; Roberts, S. A.; Brunini, V. E.; Grillet, A. M., Mechanical and Electrochemical Response of a $LiCoO_2$ Cathode Using Reconstructed Microstructures. *Electrochim. Acta* **2016**, *190*, 1-15.
39. Rahani, E. K.; Shenoy, V. B., Role of Plastic Deformation of Binder on Stress Evolution During Charging and Discharging in Lithium-Ion Battery Negative Electrodes. *J. Electrochem. Soc.* **2013**, *160*, A1153-A1162.
40. Liang, B.; Liu, Y. P.; Xu, Y. H., Silicon-Based Materials as High Capacity Anodes for Next Generation Lithium Ion Batteries. *J. Power Sources* **2014**, *267*, 469-490.
41. Takamura, T.; Ohara, S.; Uehara, M.; Suzuki, J.; Sekine, K., A Vacuum Deposited Si Film Having a Li Extraction Capacity over 2000 mAh/g with a Long Cycle Life. *J. Power Sources* **2004**, *129*, 96-100.
42. Maranchi, J. P.; Hepp, A. F.; Kumta, P. N., High Capacity, Reversible Silicon Thin-Film Anodes for Lithium-Ion Batteries. *Electrochem. Solid-State Lett.* **2003**, *6*, A198-A201.
43. Ding, B.; Wu, H.; Xu, Z. P.; Li, X. Y.; Gao, H. J., Stress Effects on Lithiation in Silicon. *Nano Energy* **2017**, *38*, 486-493.
44. Malyi, O.; Kulish, V. V.; Tan, T. L.; Manzhos, S., A Computational Study of the Insertion of Li, Na, and Mg Atoms into Si(111) Nanosheets. *Nano Energy* **2013**, *2*, 1149-1157.
45. Ruffo, R.; Hong, S. S.; Chan, C. K.; Huggins, R. A.; Cui, Y., Impedance Analysis of Silicon Nanowire Lithium Ion Battery Anodes. *J. Phys. Chem. C* **2009**, *113*, 11390-11398.
46. Ho, C.; Raistrick, I. D.; Huggins, R. A., Application of A-C Techniques to the Study of Lithium Diffusion in Tungsten Trioxide Thin Films. *J. Electrochem. Soc.* **1980**, *127*, 343-350.

Table of contents graphic